STM JOURNALS

Journal of
Polymer & Composites

https://journals.stmjournals.com/jopc

ISSN: 2a321-2810 (Online)
ISSN: 2321-8525 (Print)
Volume 14, Issue 5, 2026
September–October
DOI (Journal): 10.37591/JoPC

Research JoPC

Tailoring the Compressive Behavior of Tetrachiral Auxetic Structures Through FDM Process-Parameters

Supriya R. Tambe[1,]*, Ravindra R. Navthar[2]

Abstract

This research evaluates how fused deposition modeling (FDM) fabrication process parameters affect the compressive behavior of tetrachiral auxetic structures created from Polylactic Acid (PLA). Auxetic materials have several useful properties, including reversible deformation and high-energy absorbing capabilities, which are beneficial to creating ultra-lightweight structural, protective, and shock-resistance designs. Among the available auxetic topologies, the tetrachiral configuration is particularly attractive for engineering use, because its rotation-dominated node–ligament deformation gives a negative Poisson's ratio that remains stable over a wide strain range, its four-fold symmetry gives a nearly isotropic in-plane response suited to sandwich cores under poorly defined loading, and its long compressive plateau prior to densification favors efficient energy absorption. Three key FDM process-parameters – layer thickness, raster width and printing speed – were selected to evaluate their effects on compressive strength, stiffness and specific energy absorption (SEA). The experimental design was developed using the Taguchi method with an L9 orthogonal array, enabling efficient investigation of multiple process variables while reducing the number of experimental trials. Nine tetrachiral PLA specimens were fabricated under different combinations of processing conditions and subjected to quasi-static uniaxial compression testing in accordance with ASTM C365. The experimental results were analyzed using signal-to-noise (S/N) ratios to determine the optimal parameter combinations, while analysis of variance (ANOVA) was employed to quantify the statistical significance and relative contribution of each process parameter. The findings reveal that layer thickness is the most influential parameter affecting all three mechanical responses, whereas raster width and printing speed demonstrate comparatively smaller but appreciable effects. Overall, reductions in layer thickness and increases in raster width improved the compressive behavior of the fabricated structures. The minimum layer thickness of 0.15 mm consistently produced the highest compressive strength, stiffness and SEA because of enhanced interlayer bonding and reduced internal defects. These findings provide valuable practical guidance for optimizing FDM parameters and manufacturing tetrachiral auxetic structures with improved load-bearing capacity, structural rigidity and energy-absorption performance.

***Author for Correspondence**
Supriya R. Tambe
E-mail id: gadhesupriya@gmail.com

[1]Ph.D., Research Scholar, Department of Mechanical Engineering, Dr. Vithalrao Vikhe Patil College of Engineering, Ahilyanagar, Maharashtra, India
[2]Professor, Department of Mechanical Engineering, Dr. Vithalrao Vikhe Patil College of Engineering, Ahilyanagar, Maharashtra, India

Received Date: July 09, 2026
Accepted Date: July 22, 2026
Published Date: August 02, 2026

Citation: Supriya R. Tambe, Ravindra R. Navthar. Tailoring the Compressive Behavior of Tetrachiral Auxetic Structures Through FDM Process-Parameters. Journal of Polymer & Composites. 2026; 14(5): 58–70p.

Keywords: Compressive strength, fused deposition modeling, layer height, raster width, printing speed

INTRODUCTION

Auxetic materials are a special class of materials that possess a negative Poisson's ratio (NPR) as opposed to the positive values seen in conventional materials. Therefore, auxetic materials display an anomalous expansion and contraction in the dimensions along the transverse direction for tensile and compressive loads, respectively, as depicted in Figure 1 [1].

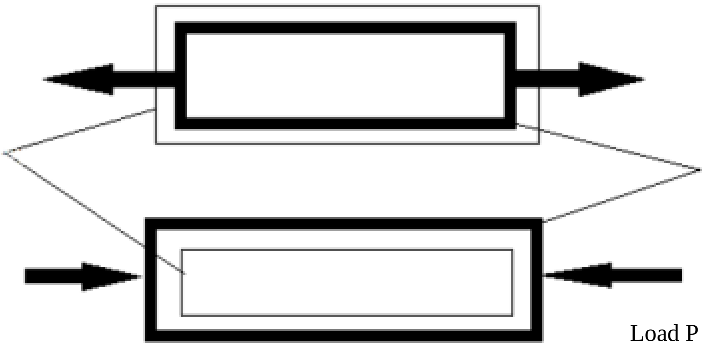

Figure 1. Behavior of auxetic structures under tensile and compressive loads.

Because of its greater strength-to-weight ratio and capacity to absorb energy, cellular structures are widely used in a variety of industries, including the automotive, sports, aerospace, and medical sectors. Auxetic structure is a newly created cellular structure with better mechanical qualities. Auxetic structures have a negative Poisson's ratio because of their special structural geometry. Because of its NPR, auxetic structures contract laterally under compression force, in contrast to conventional structures that expand. They have exceptional mechanical qualities, including enormous shear modulus, high fracture toughness, synclastic form under bending moment, and distinctive acoustic qualities. Automobile crash boxes, sturdy shock absorbers, fasteners, air seat cushions, sound absorbers, air filters, and mass filters are just a few of the many uses for auxetic structures. Auxetic structures can be re-entrant, tetrachiral, anti-tetrachiral, trichiral, anti-trichiral, hexachiral, star-shaped, lozenge grid, double arrowhead structures, and more. Because the load is conveyed to the ligament by rotating nodes, chiral configurations have a unique deformation process among these structures. Trichiral, tetrachiral, and hexachiral structures are those that have three, four, or six ligaments attached to a single node, respectively. Chiral structures are those in which nodes are connected on the opposing side of the structure [2].

Among the various auxetic topologies listed above, the tetrachiral configuration is of particular interest for engineering applications for five reasons. First, its deformation is rotation-dominated: the compressive load carried by the ligaments is converted into a torque on the cylindrical nodes, so that the ligaments wind around the nodes and the negative Poisson's ratio is generated by a geometric rotation mechanism rather than by hinge bending alone. The auxetic response is, therefore, comparatively stable and almost independent of the applied strain over a wide deformation range, in contrast to re-entrant honeycombs, whose Poisson's ratio changes markedly as the re-entrant angle closes. Second, because four ligaments are arranged around each node, the unit cell possesses four-fold symmetry, so the in-plane response is essentially isotropic, and the structure carries load equally well along the two principal directions – a valuable property for sandwich cores that experience multi-axial or poorly defined loading. Third, the progressive winding of the ligaments, followed by densification, produces a long and comparatively flat stress plateau, which is precisely the response required for efficient energy absorption in crash boxes, protective padding, helmet liners and blast-resistant panels.

Fourth, the negative Poisson's ratio draws material towards the point of loading instead of away from it, which improves indentation, impact and fracture resistance, while the synclastic (dome-like) curvature associated with a negative Poisson's ratio allows flat panels to be formed into doubly curved shells without wrinkling or darting – an advantage for aerospace fuselage panels and automotive body panels. Fifth, the mechanical behavior of the tetrachiral cell is highly tunable: the stiffness, strength and energy absorption can be adjusted over a wide range simply by changing the node radius-to-ligament-length ratio (r/L) and the ligament slenderness (t/L), without changing the base material. Together with the fact that the open, curved cell geometry is readily produced by additive manufacturing but is very difficult to obtain by conventional processing, these characteristics make tetrachiral lattices strong candidates for lightweight sandwich cores, energy-absorbing crash structures, morphing and deployable components, vibration and acoustic isolators, fasteners, filters, and biomedical devices such as stents and prostheses [1–4]. It is this combination of stable auxeticity, in-plane isotropy, high specific energy absorption and geometric tunability that motivates the present study of how the structure's compressive performance can be further tailored through the fabrication process itself.

The fabrication technique's process parameters have an impact on the structure's mechanical properties. It is challenging to fabricate these structures using conventional manufacturing methods [5]. The creation of such intricate structures has been made easier by recent developments in additive manufacturing (AM) techniques [6]. Filament is used to supply a variety of polymeric materials. After additional heating, the extruder deposits it on the print bed. Layer by layer, the components are made. The main process variables that impact the structure's compressive qualities include layer height, print temperature, print speed, raster angle, raster width, contour width, and airgap [7]. The mechanical characteristics of additively generated polymer parts have been studied by several researchers. Layer height, raster angle, and air gap were found to have a substantial impact on the parts' elasticity [8]. By altering the layer height and raster angle, Wu et al. [9] compared the mechanical characteristics of acrylonitrile-butadiene-styrene (ABS) and polyether ether ketone (PEEK) materials. They found that as layer height grows, so does the structure's strength. Mohamed et al. [10] investigated how process variables affected the standard size polymer parts' dynamic properties. According to their findings, the most important process parameters affecting the part's modulus and dynamic viscosity are layer height, air gap, and shell count. The impact of layer height, line direction, and shell count on the strength of ABS and PLA re-entrant structures was examined by Vyavahare and Kumar (2021) [11]. According to their findings, the variation in layer height is proportionate to the strength of the structure.

A review of the literature reveals that numerous attempts have been made to look into how process parameters affect the mechanical characteristics of ME-fabricated parts of standard sizes that are advised by the American Society for Testing and Materials (ASTM) and the International Organization for Standardization (ISO) such as ISO 178, ASTM D638, ASTM D695, and ASTM D790 [2]. Researchers have examined how geometric parameters affect the mechanical characteristics of PET-G polymeric materials' tetrachiral auxetic structures [3]. Nevertheless, relatively little research has been published on the impact of material extrusion process parameters on the mechanical characteristics of tetrachiral structures. This study examines how process parameters affect the tetrachiral structure's compressive strength (σ), stiffness, and specific energy absorption (SEA).

MATERIALS AND METHODS

The current work's methodology consists of computer-aided design (CAD) modeling of components, experiment design, specimen production, response measurement, and process parameter optimization. Later in the study, each phase is briefly explained.

Selection of Chiral Structure

Figure 2 depicts the tetrachiral structure's unit cell. Node radius (r), ligament thickness (t), and ligament length (L) are some of the design characteristics that affect the structure's mechanical performance. The literature review determines the final geometry of the tetrachiral auxetic structure [3]. CATIA software is used to construct tetrachiral auxetic structures. The auxetic structure's representative computer-aided design (CAD) model with a tetrachiral configuration is displayed in Figure 2. The specimen measures 70 × 60 × 20 mm³. Geometric parameters are r-radius at node = 4 mm, t-thickness of ligament = 2 mm, L-length of ligament = 8 mm. Compression testing of cellular core structure is only permitted if the specimen's cross-sectional area is smaller than 10,000 mm², according to ASTM C365. As a result, the specimen's overall size complies with ASTM C365 requirements.

Selection of Materials

For part fabrication, engineering-grade polymers – like polylactic acid (PLA), acrylonitrile butadiene styrene (ABS), polycarbonate (PC), PC-ABS, and PC-ISO – are frequently utilized. PLA (polylactic acid) is the most widely used substance that can be printed using FDM technology. PLA is widely used, especially in hobbyist applications and for making early iterations of functional prototypes, due to its simplicity of printing and the variety of colors that are available. Additionally, this substance is the most extensively used printing medium in the world due to its low cost, biodegradability, and the wealth of research on it [12]. The structure is made of PLA (Table 1).

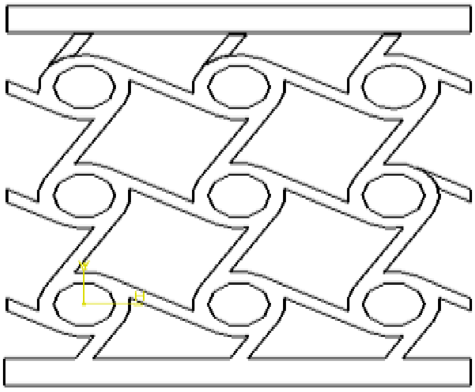

(a)

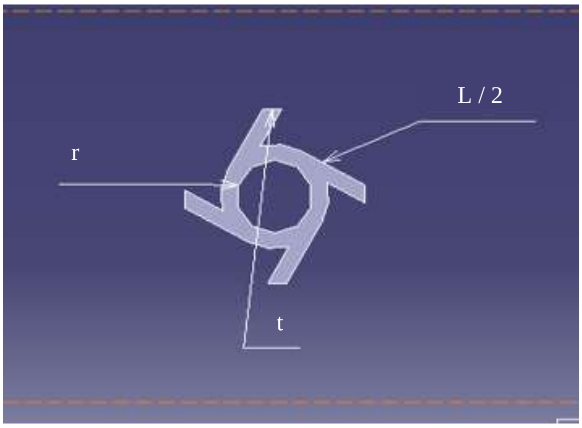

(b)

Figure 2. Unit cell of tetrachiral structure with design parameters.

Table 1. Material properties of PLA [11].

Material	Density (gm/cm^3)	Modulus of elasticity (GPa)	Poisson's ratio	Yield strength σ_y
PLA	1.252	3.5	0.36	20

FDM Process-Parameters

The right choice of process parameters is essential to the additive manufacturing process's success. For production engineers, determining the ideal process conditions is a crucial task. It is crucial for ensuring product quality, increasing dimensional accuracy, preventing excessive waste and scraps, increasing productivity rates, and cutting down on manufacturing time and expense. FDM is a complicated process with many competing characteristics that affect the material properties and part quality, making it difficult to choose the ideal parameters. Appropriate process parameter selection is responsible for the manufactured part's mechanical qualities and quality [10]. Three control factors of FDM, i.e., layer thickness, raster width, and printing speed, are taken in the present investigation, depending upon the materials, machine and literature.

Experimental Design

For design of experiments, Taguchi's orthogonal array L9 is used, as there are 3 process parameters at 3 levels each [13]. Layer thickness, print speed and raster width are the process parameters, which are selected for experimental investigation. Levels of process parameters are decided based on the literature review. The responses are compressive strength, stiffness, and SEA. A total of 9 experiments are conducted for compression testing of the structures. The levels of process parameters and experimental design are given in Tables 2 and 3, respectively.

Table 2. Process parameters and their range.

Process parameter	Level 1	Level 2	Level 3
Layer thickness (mm)	0.15	0.25	0.35
Print speed (mm/s)	45	55	65
Raster width (mm)	0.35	0.45	0.55

Table 3. Process parameter for each run.

Run	Layer thickness (mm)	Print speed (mm/s)	Raster width (mm)	Built time
1	0.15	45	0.35	5 H 35 Min
2	0.15	55	0.45	4 H 55 Min
3	0.15	65	0.55	4 H 35 Min
4	0.25	45	0.45	3 H 23 Min
5	0.25	55	0.55	3 H 11 Min
6	0.25	65	0.35	3 H 35 Min
7	0.35	45	0.55	2 H 28 Min
8	0.35	55	0.35	2 H 42 Min
9	0.35	65	0.45	2 H 38 Min

Fabrication of Specimens

The cellular core is positioned between two plates (top and bottom) due to the structure's architecture. To minimize plate deformation during testing, both plates are maintained at a thickness of 5 mm. Because a tetrachiral unit cell has one cylinder and four ligaments, the entire structure exhibits symmetry in the X and Y directions. Figure 3 shows these manufactured configurations. The example is printed using PLA feedstock material. CATIA software is used to produce the CAD model. An STL file is created from the 3D CAD model. The CAD model's stereo-lithography (STL) file is sliced using Cura software (M/s Ultimaker). Slicing software creates the G-codes by slicing the CAD model based on process parameters. The machine is then fed the G-code files. The specimens were made using a larger Pratham 3.0 3D printer with a build volume of 300 × 300 × 300 mm. Table 4 lists the values of constant process parameters employed in the production of all configurations. Nine different tetrachiral auxetic structure configurations are produced on an FDM machine using the experiment design (Table 3, Figure 3.)

Table 4. Constant process parameters of FDM.

Parameter	Value
Build orientation	Flat (XY plane).
Bed temperature	60°C.
Infill percentage	100%.
Printing temperature	210°C.
Raster angle	0.
Nozzle diameter	0.4 mm.

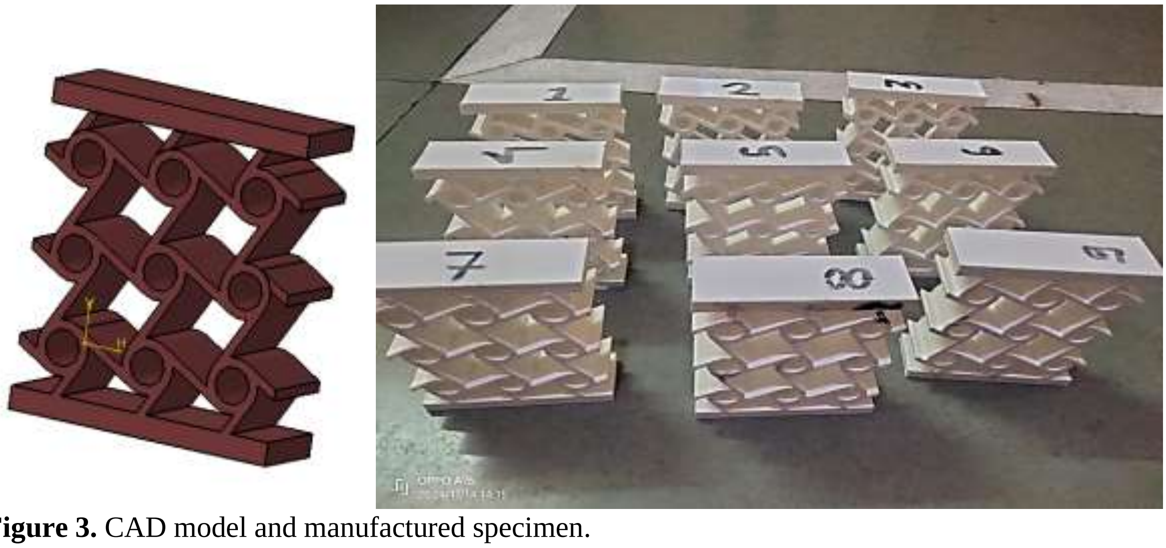

Figure 3. CAD model and manufactured specimen.

MEASUREMENT OF RESPONSES OF AUXETIC STRUCTURES

A universal testing machine is used to conduct quasi-static uniaxial compressive tests. Model: STS-248 with a 1000 kg load cell. Five millimeters per minute is the cross-head speed [14]. Stiffness, energy absorbed by structures, and load-displacement curves are evaluated. Tests are carried out in accordance with ASTM C365, a standard test procedure for sandwich core flatwise compression properties. Because the bonding strength between each layer of the structure may be measured while loading in the Y direction, compressive load is applied to the structures along the Y-axis, or perpendicular to the construction direction. The specimen and machine setup for the compression tests is shown in Figures 4 and 5. Every specimen is evaluated at a consistent rate of 5 mm/min in accordance with the experimental design. Until the specimen reaches the densification stage, the compression load is applied. For every tested specimen, the machine's software generates a load-displacement curve. These curves are post-processed to determine desired responses. Compressive strength is defined as the ratio of the applied load to the initial cross-sectional area of the structure. The ratio of stress to strain determines compressive stiffness, often known as the modulus of compression. The total energy absorbed during compression is determined for each structure by calculating area under the stress–strain curve, Equation (1) [2]. SEA of auxetic structure is calculated by using Equation (2). Relative density of tetrachiral structure is given by Equation (4) [4]. Relative density of structure depends on the geometric parameter of the structure. It varies as the dimensions of the structure vary. Density of (PLA) bulk material is 1.252 gm/cm³.

$$\text{Compressive Strength}(\sigma) = \frac{Load}{Area} \tag{1}$$

$$W = \int_0^{\varepsilon} \sigma(\varepsilon)\, d\varepsilon \tag{2}$$

$$SEA = \frac{W}{(\Delta\rho * \rho s)} \tag{3}$$

$$\text{Relative density of structure} = \Delta\rho = 2\left(\frac{t}{l}\right)\left(\frac{1+\pi\left(\frac{r}{l}\right)}{1+4\left(\frac{r}{l}\right)^2}\right) \tag{4}$$

Δρ = Relative density of structure. ρs = density of bulk material.

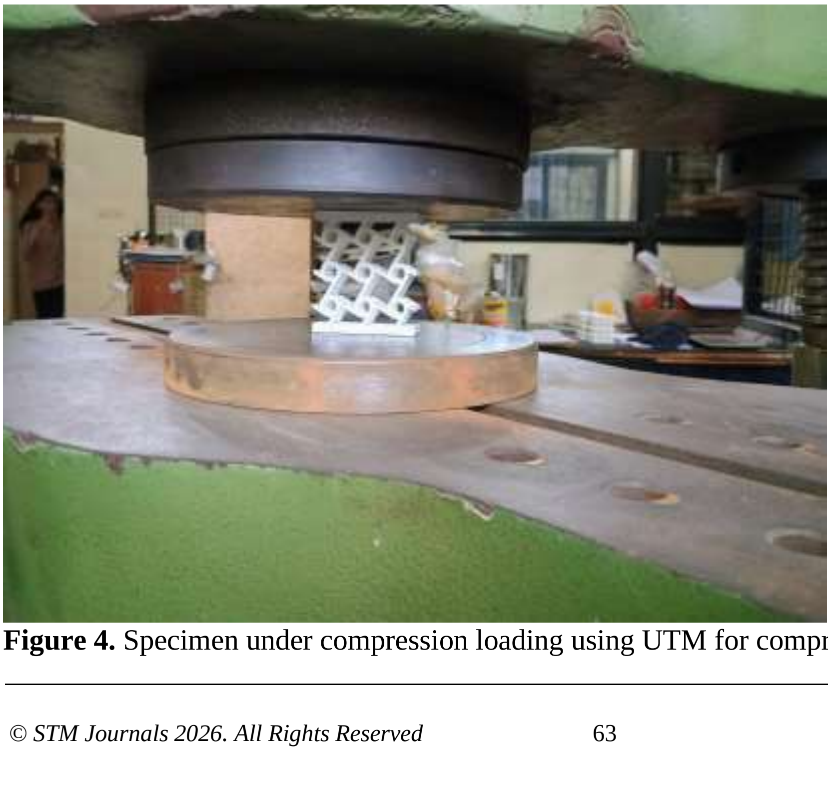

Figure 4. Specimen under compression loading using UTM for compression loading.

Journal of Polymer & Composites
Volume 14, Issue 5
ISSN: 2321-2810 (Online) ISSN: 2321-8525 (Print)

Figure 5. Tetrachiral AUXETIC STRUCTURES after compression testing.

DEFORMATION MECHANISM

As seen in Figure 6, under compressive loading, force is applied perpendicular to the face plate and subsequently transferred to the ligaments. Torque is applied to the circular parts as the load passes through the ligaments. Deformation results from the ligaments wrapping around the circular parts. Densification of the structure occurs because of this deformation, where the first layer of unit cells occupies the space of second layer unit cells and the second layer occupies the space of third layer unit cells.

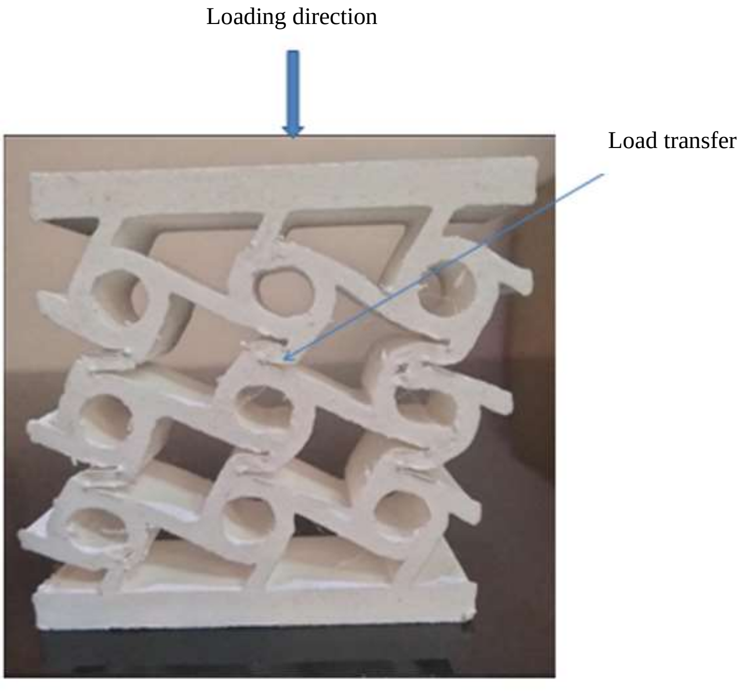

Figure 6. Deformation of tetrachiral auxetic structure.

RESULTS AND DISCUSSION

The compressive strength, stiffness and specific energy absorption obtained from the nine compression experiments are summarized in Table 5. Each response was extracted from the corresponding load–displacement curve using the procedure described in Section under the Heading "Measurement of Responses of Auxetic Structures". The data were then analyzed using the Taguchi signal-to-noise (S/N) ratio method and analysis of variance (ANOVA) to quantify the influence and the relative contribution of each process parameter to the measured responses, as presented in the following subsections.

Table 5. Experimental results of compression tested specimen.

Run	Layer thickness (mm)	Print speed (mm/s)	Raster width (mm)	Strength (MPa)	Stiffness (MPa)	SEA (J/gm)
1	0.15	45	0.35	1.525	18.43	0.2067
2	0.15	55	0.45	2.175	27.06	0.2441
3	0.15	65	0.55	2.8	28.49	0.4604
4	0.25	45	0.45	1.85	19.87	0.2210
5	0.25	55	0.55	0.8	16.06	0.1053
6	0.25	65	0.35	1.775	19.23	0.1805
7	0.35	45	0.55	2.25	27.35	0.2709
8	0.35	55	0.35	1.65	17.67	0.1605
9	0.35	65	0.45	1.39	19.23	0.1460

Signal-to-Noise (S/N) Ratio Analysis

Because high strength, stiffness and specific energy absorption are all desirable, the larger-the-better S/N ratio was used, defined as $S/N = -10 \log_{10}[(1/n) \Sigma(1/y^2)]$, where y is the measured response and n is the number of observations per run. The mean S/N ratio was computed for each factor at each level; the factor with the largest range (delta) between levels has the greatest influence on the response, and the level giving the highest S/N ratio is the optimal level. The response tables for the three responses are given in Tables 6–8 (factor levels correspond to the values listed in Table 2).

Table 6. Response table for S/N Ratios – compressive strength (larger-the-better).

Factor	Level 1	Level 2	Level 3	Delta	Rank
Layer thickness	6.45	2.80	4.75	3.66	1
Print speed	5.35	3.05	5.60	2.54	2
Raster width	4.33	4.98	4.68	0.65	3

Table 7. Response table for S/N ratios – stiffness (larger-the-better).

Factor	Level 1	Level 2	Level 3	Delta	Rank
Layer thickness	27.68	25.25	26.45	2.43	1
Print speed	26.67	25.90	26.82	0.92	3
Raster width	25.31	26.76	27.32	2.00	2

Table 8. Response table for S/N ratios – specific energy absorption (Larger-the-better).

Factor	Level 1	Level 2	Level 3	Delta	Rank
Layer thickness	−10.89	−15.85	−14.65	4.95	1
Print speed	−12.72	−15.90	−12.77	3.18	2
Raster width	−14.82	−14.03	−12.54	2.27	3

The response tables show that layer thickness has the largest delta, and hence the strongest influence, for all three responses. Level 1 (0.15 mm) gives the highest S/N ratio in every case, confirming that the finest layer thickness is optimal. Raster width is the second most influential factor for stiffness, while print speed ranks second for strength and specific energy absorption.

Analysis of Variance (ANOVA)

ANOVA was carried out on the measured responses to quantify the percentage contribution of each process parameter. In the L9 array the three factors consume six degrees of freedom, leaving two degrees of freedom for the residual (error) term. The results are given in Tables 9–11, where SS is the sum of squares, DOF the degrees of freedom, MS the mean square, F the variance ratio (MS_{factor}/MS_{error}) and P the percentage contribution.

Table 9. ANOVA for compressive strength.

Source	DOF	SS	MS	F	P (%)
Layer thickness	2	0.7242	0.3621	0.51	27.72
Print speed	2	0.3235	0.1617	0.23	12.38
Raster width	2	0.1350	0.0675	0.09	5.17
Error	2	1.4297	0.7149	–	54.73
Total	8	2.6125	–	–	100

Table 10. ANOVA for stiffness.

Source	DOF	SS	MS	F	P (%)
Layer thickness	2	59.055	29.527	0.88	32.69
Print speed	2	7.028	3.514	0.10	3.89
Raster width	2	47.200	23.600	0.70	26.13
Error	2	67.362	33.681	–	37.29
Total	8	180.645	–	–	100

Table 11. ANOVA for specific energy absorption.

Source	DOF	SS	MS	F	P (%)
Layer thickness	2	0.03111	0.01555	1.24	36.66
Print speed	2	0.01335	0.00667	0.53	15.73
Raster width	2	0.01537	0.00769	0.62	18.12
Error	2	0.02502	0.01251	–	29.49
Total	8	0.08485	–	–	100

The ANOVA confirms the S/N ranking: layer thickness is the largest single contributor to every response (about 28% for strength, 33% for stiffness and 37% for specific energy absorption). Raster width is the second largest contributor for stiffness (about 26%), while print speed contributes less than about 16% in all cases. It should be noted that, because only one specimen was tested per run, the error term has only two degrees of freedom and is relatively large (up to about 55% for strength); consequently, the F values do not reach the critical value for significance at the 95% confidence level. The percentage contributions should, therefore, be interpreted as indicating the relative influence of each factor rather than as a formal test of significance, and replicating experiments are recommended to obtain a firmer statistical basis (see Section under the Heading "Effectiveness of the Optimization Approach").

Effect of Process Parameters and Deformation Behavior

The S/N and ANOVA results consistently identify layer thickness as the dominant process parameter, and the finest layer thickness of 0.15 mm produced the highest values of all three responses. A smaller layer thickness increases the number of deposited layers for a given specimen height and improves the geometric fidelity of the curved ligaments and cylindrical nodes of the tetrachiral cell. The load is then transferred more uniformly around the nodes, with fewer stress-concentrating inter-bead defects. Coarser layers (0.35 mm) reduce the resolution of the ligament–node junctions and introduce larger internal voids, which lowers the load-bearing capacity.

Raster width is the second most influential factor for stiffness and increasing it from 0.35 mm to 0.55 mm raised the S/N ratios for stiffness and specific energy absorption. Wider rasters deposit more material per pass and reduce the number of bead-to-bead interfaces and internal voids within the ligaments, increasing the effective cross-section that resists compression. Print speed had a comparatively minor and less systematic effect: its influence on strength and SEA was non-monotonic, which is consistent with two competing mechanisms, namely that higher speeds shorten the time available for inter-bead fusion (tending to weaken bonding) while also reducing thermal dwell and warping.

To describe the trends between the FDM process-parameters and the compressive strength explicitly, the mean measured response at each factor level is given in Table 12. Three distinct trends are observed.

Table 12. Mean response values at each factor level.

Factor	Level	Mean compressive strength (MPa)	Mean stiffness (MPa)	Mean SEA (J/gm)
Layer thickness (mm)	0.15	2.167	24.66	0.3037
	0.25	1.475	18.39	0.1689
	0.35	1.763	21.42	0.1925
Print speed (mm/s)	45	1.875	21.88	0.2329
	55	1.542	20.26	0.1700
	65	1.988	22.32	0.2623
Raster width (mm)	0.35	1.650	18.44	0.1826
	0.45	1.805	22.05	0.2037
	0.55	1.950	23.97	0.2789

i. *Layer Thickness* – compressive strength. The mean compressive strength falls sharply from 2.167 MPa at 0.15 mm to 1.475 MPa at 0.25 mm, a reduction of about 32%, and then recovers partially to 1.763 MPa at 0.35 mm. The trend is thus a decreasing but non-monotonic one, with the finest layer clearly giving the highest strength. The dominant drop between 0.15 mm and 0.25 mm follows from the larger number of thin layers at the fine setting, which raises the total bonded interfacial area, improves the geometric fidelity of the curved ligaments and cylindrical nodes, and reduces inter-bead voids. The partial recovery at 0.35 mm is attributed to the larger cross-sectional area of each individual extruded bead at coarse layer settings, which increases the load-bearing area within a ligament even though fewer interfaces are formed; the same non-monotonic pattern is visible in the S/N response of Table 6.

ii. *Raster Width* – compressive strength. This trend is monotonically increasing. The mean strength rises steadily from 1.650 MPa at 0.35 mm to 1.805 MPa at 0.45 mm and 1.950 MPa at 0.55 mm, an overall gain of about 18%. Wider rasters deposit more material per pass and reduce both the number of bead-to-bead interfaces and the internal porosity within a ligament of fixed thickness, so the effective load-bearing cross-section increases. This is the most consistent of the three trends, although raster width has the smallest magnitude of effect on strength (5.17% contribution in Table 9).

iii. *Print Speed* – compressive strength. This trend is non-monotonic and V-shaped: the mean strength decreases from 1.875 MPa at 45 mm/s to 1.542 MPa at 55 mm/s and then rises to 1.988 MPa at 65 mm/s. The behavior reflects two competing mechanisms. An increase in speed shortens the time available for polymer inter-diffusion at the bead interface and, therefore, weakens interlayer bonding, but it also shortens the thermal dwell time and so reduces residual thermal stress and warping in the slender ligaments. The minimum at 55 mm/s coincides with the level at which the anomalous Run 5 was performed, so part of this dip is attributable to specimen scatter rather than to purely physical effect.

Overall, the trend between the FDM parameters and compressive strength may be summarized as follows: the compressive strength increases as the layer thickness decreases and as the raster width increases, whereas the print speed has a weaker and non-monotonic influence. The same directional trends were obtained for stiffness and for specific energy absorption, which indicates that the settings favoring good interlayer bonding also favor energy absorption. The highest strength in the entire matrix, 2.8 MPa (Run 3), was obtained with the finest layer thickness (0.15 mm) combined with the widest raster (0.55 mm), while the lowest, 0.8 MPa (Run 5), occurred at an intermediate layer thickness of 0.25 mm. The two extremes differ by a factor of 3.5, which shows that the FDM process settings alone can alter the compressive strength of a nominally identical tetrachiral geometry by more than 200%.

The deformation mechanism described in the Section under the Heading "Deformation Mechanism", in which the ligaments wind around the rotating cylindrical nodes and the structure progressively densifies, was observed in all specimens. One data point, Run 5 (0.25 mm, 55 mm/s, 0.55 mm), gave an unexpectedly low strength of 0.8 MPa that deviates from the general trend. Such outliers are commonly caused by localized printing defects, for example under-extrusion or a weak node–ligament junction, and they contribute to the relatively large residual term in the ANOVA. Because only a single specimen was tested per run, this scatter cannot be separated from genuine parameter effects, which again motivates replicate testing.

These trends are broadly consistent with previous FDM studies of auxetic cellular structures. Vyavahare and Kumar [11, 14] reported that layer height and raster parameters strongly influence the compressive response of re-entrant PLA and ABS structures, and Teraiya et al. [2] found design and process parameters to govern the behavior of anti-tetrachiral structures. The present work extends these observations to tetrachiral PLA structures and quantifies, through ANOVA, the dominant role of layer thickness.

Determination of Optimal Parameters

Table 13 summarizes the optimal parameter levels obtained from the S/N analysis for each response. A layer thickness of 0.15 mm is optimal for all three responses. The optimal print speed and raster width differ slightly between responses: strength is maximized at 0.15 mm/65 mm/s/0.45 mm, stiffness at 0.15 mm/65 mm/s/0.55 mm, and specific energy absorption at 0.15 mm/45 mm/s/0.55 mm. Where a single compromise setting is required for a structure that must simultaneously provide high strength, stiffness and energy absorption, a layer thickness of 0.15 mm combined with the larger raster width of 0.55 mm is recommended, with the print speed selected according to the property of greatest importance. A confirmation experiment at the selected optimum, including replicate specimens, should be carried out to validate the predicted improvement.

Table 13. Optimal process-parameter levels from S/N analysis.

Response	Layer thickness (mm)	Print speed (mm/s)	Raster width (mm)
Compressive strength	0.15	65	0.45
Stiffness	0.15	65	0.55
Specific energy absorption	0.15	45	0.55

Effectiveness of the Optimization Approach

The effectiveness of the Taguchi optimization was assessed in three ways: by the experimental economy it delivered, by the improvement predicted at the identified optimum relative to the experimental matrix, and by an internal validation of the additive model against a combination that was actually tested.

A full factorial study of three parameters at three levels would require 27 experiments. The L9 orthogonal array produced the same main-effect information from only 9 runs, a reduction of 67% in fabrication and testing effort. Given that the build time of a single specimen ranged from 2 h 28 min to 5 h 35 min (Table 3), this economy is a substantial practical benefit and is the first measure of the method's effectiveness.

The improvement delivered by the optimization was then quantified using the Taguchi additive model, in which the S/N ratio at the optimum is predicted as the overall mean S/N ratio plus the sum of the deviations of the optimal level of each factor from that mean. Converting the predicted S/N ratio back into the physical response through $y = 10^{(S/N)/20}$ gives the predicted optimum values listed in Table 14. Relative to the mean of the nine experimental runs, the optimization predicts an improvement of 34.7% in compressive strength (from 1.80 MPa to 2.43 MPa), 29.5% in stiffness (from 21.49 MPa to 27.83 MPa) and 68.3% in specific energy absorption (from 0.2217 J/gm to 0.3731 J/gm). Measured against the poorest-performing combination in the matrix (Run 5), the predicted gains are considerably larger: 203% in strength, 73% in stiffness and 254% in SEA. The method is, therefore, effective in the practical sense that, from only nine trials, it identifies parameter settings that raise all three compressive responses well above the average performance of the matrix, and it does so for all three responses simultaneously through a common layer thickness of 0.15 mm.

Table 14. Effectiveness of the Taguchi optimization for the three compressive responses.

Response	Mean of the nine runs	Poorest run (Run 5)	Predicted at optimum	Improvement over mean (%)	Improvement over Run 5 (%)
Compressive strength (MPa)	1.802	0.800	2.426	34.7	203.3
Stiffness (MPa)	21.49	16.06	27.83	29.5	73.3
Specific energy absorption (J/gm)	0.2217	0.1053	0.3731	68.3	254.3

An internal check on the reliability of the additive model is available for stiffness, because the optimum identified for that response (0.15 mm/65 mm/s/0.55 mm) coincides with Run 3 of the experimental matrix. The model predicts 27.83 MPa at this setting, whereas the measured value is 28.49 MPa, an error of only 2.3%. This close agreement indicates that the additive main-effect model represents the compressive behavior of the tetrachiral structure well, and that the levels selected by the S/N analysis are physically meaningful rather than artefacts of the design. It is also noted that Run 3 gave the highest measured compressive strength (2.8 MPa) and the highest SEA (0.4604 J/gm) of all nine runs, both of which exceed the values predicted by the additive model at the corresponding optima (2.43 MPa and 0.3731 J/gm). The additive model, therefore, appears to under-predict at the corners of the design space for these two responses, which points to the presence of parameter interactions, most probably between print speed and raster width, since both govern the thermal history and the amount of material deposited per unit length. Being a main-effect design, the L9 array cannot resolve such interactions.

Finally, the effectiveness of the optimization must be judged against the statistical quality of the underlying data. As noted in the Section under the Heading "Analysis of Variance (ANOVA)", only one specimen was tested per run, so the residual term is large (up to about 55% for strength) and none of the F ratios reaches the critical value at the 95% confidence level. The percentage contributions and the optimum levels reported here should accordingly be regarded as robust and economically obtained indications of the relative importance and the direction of each parameter, rather than as statistically confirmed effects. To place the conclusions on a firmer footing, and to convert the predicted improvements of Table 14 into verified ones, confirmation experiments at the optimum settings with at least three replicate specimens per condition are recommended, together with a design capable of resolving the print speed – raster width interaction.

CONCLUSIONS

The influence of three FDM process-parameters – layer thickness, print speed, and raster width – on the compressive strength, stiffness, and specific energy absorption (SEA) of PLA tetrachiral auxetic structures was investigated experimentally using a Taguchi L9 design, followed by S/N ratio analysis and ANOVA. The main conclusions are as follows:

1. All three process parameters influence the compressive strength, stiffness and SEA of the FDM-printed PLA tetrachiral auxetic structures.
2. Layer thickness is the dominant parameter for all three responses, contributing approximately 28%, 33% and 37% to the variation in strength, stiffness and SEA, respectively, with the finest layer thickness (0.15 mm) consistently optimal.
3. Raster width is the second most influential parameter for stiffness (approximately 26%), whereas print speed has a comparatively minor effect.
4. In general, the mechanical properties improve as the layer thickness decreases and the raster width increases.
5. The Taguchi L9 approach proved both economical and effective. It reduced the experimental effort from 27 full-factorial runs to 9, and the additive model predicts improvements of

ISSN: 2321-2810 (Online) ISSN: 2321-8525 (Print)

approximately 35% in compressive strength, 30% in stiffness and 68% in SEA at the optimum settings, relative to the mean of the experimental matrix. For stiffness, where the predicted optimum coincided with a tested run, the prediction lay within 2.3% of the measured value.
6. The clearest trends with compressive strength are a pronounced decrease as the layer thickness increases from 0.15 mm to 0.25 mm (2.167 MPa against 1.475 MPa) and a monotonic increase with raster width (1.650 MPa to 1.950 MPa between 0.35 mm and 0.55 mm), while print speed exerts a weaker, non-monotonic influence. Process settings alone changed the strength of the same geometry by a factor of 3.5.
7. The relatively large residual term for strength (about 55%), together with the anomalous Run 5, indicates appreciable process scatter; replicate testing is recommended to strengthen the statistical conclusions.
8. Poisson's ratio of the structures should be measured in future work to confirm their auxetic behavior.
9. The results provide practical guidance for selecting FDM process-parameters for tetrachiral auxetic cores used in sandwich panels for automotive, aerospace, sports and biomedical applications.

Acknowledgments

The authors acknowledge the support of the Mechanical Engineering Department, Dr. Vithalrao Vikhe Patil College of Engineering, Ahilyanagar, for providing the facilities used to carry out this work.

REFERENCES

1. Joseph A, Mahesh V, Harursampath D. On the application of additive manufacturing methods for auxetic structures: A review. Adv Manuf. 2021;9(3):342–368.
2. Teraiya S, Vyavahare S, Kumar S. Anti-tetrachiral auxetic structures fabricated by material extrusion: Numerical and experimental investigation on the influence of design parameters on mechanical properties under compressive loading. Int J Mater Eng Innov. 2024;15(1):33–65.
3. Kumar S, Vyavahare S, Teraiya S, Dhakar LC. Experimental investigation on FDM fabricated tetra chiral auxetic structures under uniaxial compressive loading. In: Dave HK, Davim JP, editors. Fused Deposition Modeling Based 3D Printing. Cham, Switzerland: Springer; 2021. p. 63–83.
4. Yu X, Zhou J, Liang H, Jiang Z, Wu L. Mechanical metamaterials associated with stiffness, rigidity and compressibility: A brief review. Prog Mater Sci. 2018;94:114–173.
5. Seepersad CC, Kumar RS, Allen JK, Mistree F, McDowell DL. Multifunctional design of prismatic cellular materials. J Comput Aided Mater Des. 2004;11(2–3):163–181.
6. Alomarah A, Masood SH, Sbarski I, Faisal B, Gao Z, Ruan D. Compressive properties of 3D printed auxetic structures: Experimental and numerical studies. Virtual Phys Prototyp. 2020;15(1):1–21.
7. Vanaei H, Shirinbayan M, Deligant M, Raissi K, Fitoussi J, Khelladi S, et al. Influence of process parameters on thermal and mechanical properties of polylactic acid fabricated by fused filament fabrication. Polym Eng Sci. 2020;60(8):1822–1831.
8. Lee BH, Abdullah J, Khan ZA. Optimization of rapid prototyping parameters for production of flexible ABS object. J Mater Process Technol. 2005;169(1):54–61.
9. Wu W, Geng P, Li G, Zhao D, Zhang H, Zhao J. Influence of layer thickness and raster angle on the mechanical properties of 3D-printed PEEK and a comparative mechanical study between PEEK and ABS. Materials. 2015;8(9):5834–5846.
10. Mohamed OA, Masood SH, Bhowmik JL. Optimization of fused deposition modeling process parameters: A review of current research and future prospects. Adv Manuf. 2015;3(1):42–53.
11. Vyavahare S, Kumar S. Numerical and experimental investigation of FDM fabricated re-entrant auxetic structures of ABS and PLA materials under compressive loading. Rapid Prototyp J. 2021;27(2):223–244.
12. Montalti A, Ferretti P, Santi GM. A cost-effective approach for quality control in PLA-based material extrusion 3D printing using 3D scanning. J Ind Inf Integr. 2024;41:100660.
13. Sobih M, Elseddig Z, Almazy K, Youssef A, Sallam M. Optimization of EBW parameters for 2219 Al-alloy using grey relation method. Adv Mater Res. 2012;591–593:507–514.
14. Vyavahare S, Kumar S. Re-entrant auxetic structures fabricated by fused deposition modeling: An experimental study of influence of process parameters under compressive loading. Polym Eng Sci. 2020;60(12):3183–3196.

